Available online at www.sciencedirect.com
SCIENCE DIRECT®
Optical Materials 28 (2006) 820–824
OPTICAL Materials
www.elsevier.com/locate/optmat

Luminescence of Nd-enriched silicon nanoparticle glasses

A.N. MacDonald [a], A. Hryciw [a], Quan Li [b], A. Meldrum [a,*]

[a] Department of Physics, University of Alberta, Edmonton, Canada T6G 2J1
[b] Department of Physics, The Chinese University of Hong Kong, Shatin, NT, Hong Kong

Available online 9 November 2005

Abstract

We report on the luminescence of amorphous silicon nanocomposites doped with neodymium. Effective non-resonantly pumped emission from the neodymium ions can occur for specimens made at processing temperatures as low as 300 °C for compositions close to SiO. We discuss the emission intensities of the most important Nd transitions at wavelengths of ~800, ~900, ~1060, and ~1350 nm under non-resonant excitation (all these bands are crystal-field-split and are therefore broad). The Nd emission bands show only a weak quenching effect as a function of temperature. The results indicate that amorphous silicon nanoclusters are excellent sensitizers for the main Nd optical transitions and offer additional advantages associated with a lower-temperature fabrication procedure. Finally, we discuss optical microcavity structures containing Nd ions and silicon nanoclusters.

1. Introduction

Silicon nanocrystals are excellent sensitizers for the rare earth elements (see [1–3] and references therein.) Optical transitions in rare earth doped glasses are only weakly allowed and therefore have low excitation cross-sections ($\sim 10^{-21}$ cm^2), whereas the presence of silicon nanoparticles in the SiO_2 matrix opens up a powerful alternative excitation mechanism. Incident light is absorbed by the nanoclusters (excitation cross-sections on the order of 10^{-16} cm^2 in the blue-green part of the spectrum), followed by an efficient energy transfer to the rare earth ions. This mechanism provides two key advantages with respect to the development of practical devices: first, the excitation efficiency can be increased by orders of magnitude, and second, excitation can be broadband optical or even electrical.

Erbium-doped silicon nanocomposites have been intensively investigated and waveguide amplifiers showing net optical gain have recently been reported [4]. However, there are only a small number of studies involving other rare earth ions of technical interest such as Yb, Tb, and Nd [5–7]. Neodymium in particular is interesting for at least two reasons. First, it has an emission band in the second fiber transparency window at ~1350 nm, and second, neodymium-doped ceramics represent a classic laser amplification medium. The objects of our present investigation are therefore to characterize the optical properties of neodymium-doped silicon nanocomposites processed at low temperatures, and to explore high-Q microcavities and waveguides for gain/loss testing. Here, we report on the first aspects of our work completed to date: basic optical and microstructural characterization and the first test microcavity.

2. Experimental

Specimens were fabricated by co-evaporation of SiO and either Nd_2O_3 or Nd onto fused quartz substrates. In the first set of samples (Set A), the SiO was evaporated thermally while Nd_2O_3 was deposited by electron beam evaporation. In the second set of samples (Set B), the SiO was evaporated by electron beam evaporation while Nd was deposited thermally. Films were 100 and 200 nm thick for Set A and B, respectively, as determined by the rate monitor. Effort was made to maintain stable evaporation rates, although some minor variations were unavoidable when high-SiO rates

* Corresponding author.
E-mail address: ameldrum@phys.ualberta.ca (A. Meldrum).

0925-3467/$ - see front matter © 2005 Elsevier B.V. All rights reserved.
doi:10.1016/j.optmat.2005.09.032

were required to produce low Nd concentrations. The resulting films were subsequently annealed at temperatures between 300 and 1100 °C in $\sim 96\%N_2 + 4\%H_2$ at pressures slightly above 1 atm. This annealing atmosphere was chosen on the basis of extensive previous investigations showing the importance of hydrogen for passivating non-radiative defects (e.g., see Refs. [8–10]).

Specimens were characterized by electron microprobe analysis and transmission electron microscopy (TEM). The microprobe was operated at 3 kV to minimize beam penetration of the substrate according to electron range calculations, requiring the neodymium M-lines to be used for the analyses. The set of microprobe standards are rare earth phosphates and SiO_2 provided by the Smithsonian Institute. Standard ZAF correction techniques were applied to the microprobe data. For TEM, selected specimens were prepared by the usual cross-sectional thinning techniques, and imaging was done in high resolution and EELS modes. The photoluminescence was measured using either an Ar laser operated at 476 nm or a HeCd laser operated at 325 nm as the excitation source. The luminescence was collected using a fiber optic system, and was analyzed on either a silicon or an InGaAs CCD spectrometer whose spectral response was calibrated with a standard blackbody radiator.

3. Results and discussion

3.1. Specimen Set A

Specimens from Set A have 0.14 at.% Nd ($\sim 4 \times 10^{19}$ ions/cm^{-3}) and a Si:O ratio of 1:1.15 according to the electron microprobe results. Simulations of the X-ray distribution for a 3 kV probe beam in a 100-nm-thick SiO film show that the oxygen composition may be slightly overestimated (this is not, however, the case for the 200-nm-thick films in Set B). This concentration of Nd is the same as that used in the previous study [5]. Unexpectedly, during testing we found that the source material (Stanford Products, 99.99% Nd_2O_3) contained a significant amount of gadolinium. Gadolinium concentrations in the films were comparable to that of the neodymium. We subsequently analyzed the Smithsonian neodymium phosphate microprobe standard and found that it, too, contains several percent of Gd. The previous studies appear to have obtained Nd concentrations from the synthesis procedure only, and did not analyze for possible impurities (e.g., Ref. [5]). The electronic structure of Gd is unique among the rare earths in that the first excited state is 3.96 eV above the ground state, much higher than for Nd or for silicon nanoclusters and also above the pump wavelengths used in the present studies. Therefore, for this investigation, the Gd is inert.

The specimen was divided into eight separate pieces, which were annealed at temperatures from 400 to 1100 °C in 100° intervals. At the lower annealing temperatures, two principle luminescence bands were observed in the wavelength range of 500–1000 nm—a broad shorter-wavelength peak that is intrinsic to the Si–O matrix, and the crystal-field-split $^4F_{3/2} \rightarrow {}^4I_{9/2}$ Nd transition centered at ~915 nm (Fig. 1). The highest Nd intensity was found to occur after annealing at 400 °C. As the annealing temperature increased, the matrix peak intensity first decreased before recovering to produce a stronger luminescent band centered in the near infrared typical of silicon nanocrystals. On the other hand, the Nd emission intensity decreased monotonically and was not detectable on top of the nanocluster emission for annealing temperatures greater than 900 °C. In all specimens, a weak (non-permanent) bleaching was observed in which the emission intensity was lowered by a few percent over a period of a several minutes during laser irradiation. In order to ensure consistency, all PL results were taken after the emission intensity had stabilized.

Since these data were obtained by pumping away from any of the principal Nd absorption bands, the results show that an excitation mechanism is at work that, for a composition close to SiO, is particularly effective at the lower annealing temperatures. To illustrate the importance of the non-resonant excitation process, we also synthesized a test sample containing 0.26 at.% Nd doped into SiO_2; no Nd emission could be observed from this sample under all attempted pumping conditions, including excitations resonant with the most absorbing Nd levels (e.g., pumping at 808 nm). This observation is consistent with the low direct excitation cross-section for these transitions and with the much larger excitation cross-sections reported

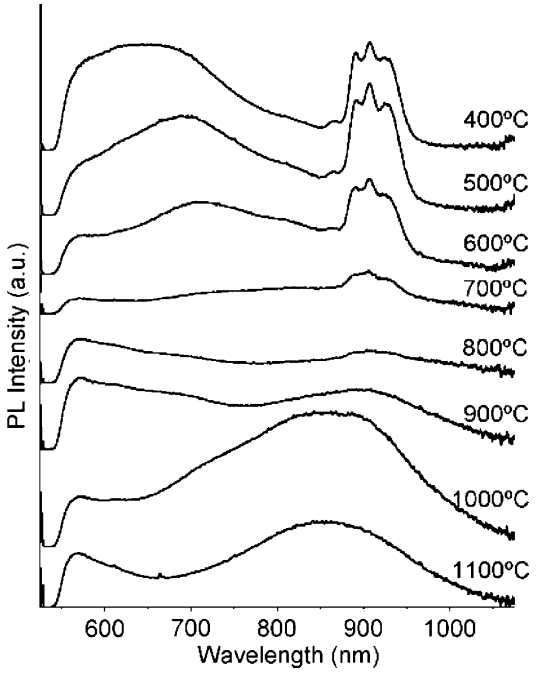

Fig. 1. Photoluminescence data for Specimen Set A (0.14 at.% Nd) for various annealing temperatures. The Si nanocluster peak shifts to longer wavelengths as the annealing temperatures increase. The Nd $^4F_{3/2} \rightarrow {}^4I_{9/2}$ peak at ~900 nm decreases with increasing annealing temperatures.

consistently, for example, in Er-doped silicon nanocomposites (see [2] and references therein).

We attribute the excitation mechanism in specimens annealed at 500 °C or lower to energy transfer from amorphous silicon nanoparticles. Indeed, we have demonstrated the existence of amorphous Si-rich clusters in SiO processed at 500 °C [11], and that the presence of these clusters is responsible for the broad PL band in the visible part of the spectrum [12]. Of particular importance is the fact that effective Nd emission can be obtained at temperatures as low as 400 °C, which makes trial device fabrication considerably easier. In the following section, we will show that this method can be extended to even lower processing temperatures.

Temperature quenching was found to be relatively minor, with the 1100 nm Nd emission band intensity decreasing by approximately 50% on heating from 4 to 285 K (Fig. 2). The quenching effect is weaker than for a high-temperature thermally-processed crystalline nanocomposite [5]. A strong temperature quenching effect is a characteristic of the undesirable back-transfer processes in which, at higher temperatures, excitations are transferred from the rare earth ions back to the Si nanoclusters (e.g., via confined carrier absorption [13]). The remarkably weak temperature dependence of the Nd emission suggests that back-transfer effects are small. On the other hand, the Si nanocluster emission intensity decreased by approximately 80% on heating from 4 to 300 K independent of the Nd emission (we observe a similar nanocluster temperature dependence in undoped samples).

The results in Figs. 1 and 2 are encouraging, but the presence of a pronounced nanocluster luminescence peak suggests that the samples may not be optimized. At the lowest Nd concentrations the emission intensity should be proportional to the Nd concentration and, as observed in Specimen Set A, the nanocluster emission will still be present. At higher Nd levels, concentration quenching processes become important and the Nd emission should decrease, as observed in laser glass [14]. In other words, there should be enough Nd to optimize the transfer from the silicon nanoclusters but not so much that concentration quenching becomes significant. Therefore, the results suggest that increased Nd concentrations may lead to a stronger emission in the present materials. In Specimen Set B, therefore, the Nd concentration was varied in order to optimize the emission intensity.

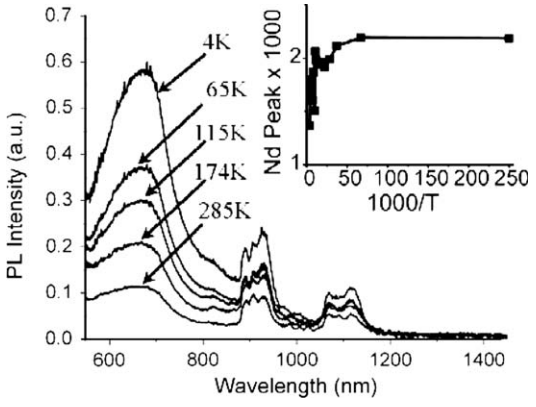

Fig. 2. Photoluminescence data for Specimen Set A (0.14 at.% Nd) at temperatures from 4 to 285 K. Data from two spectrometers, infrared and visible, are stitched together at approximately 950 nm to display a greater range. Inset shows the fitted intensity of the second Nd peak at 1100 nm as a function of $1000/T$ (the line is a guide to the eye).

Table 1
Electron microprobe results for Specimen Set B

Nd	Si	O	Al
Atomic % from microprobe			
1.720	48.928	49.337	0.015
0.920	49.514	49.566	0.000
0.602	49.246	50.145	0.007
0.474	49.792	49.723	0.011
0.442	49.806	49.713	0.038
0.493	49.815	49.686	0.007

All data are normalized to 100%.

3.2. Set B

Specimen Set B was produced using metallic Nd in the source, since highly stable evaporation rates could be obtained and the impurity concentration was found to be smaller. The electron microprobe results for Specimen Set B are shown in Table 1. In this case, the starting material (nominally 99.99% Nd) has small but detectable impurities principally of aluminum (less than 0.1 at.%), while the concentration of Gd was below detection limits. For these evaporation conditions, the Si:O ratio was very close to 1:1 (effectively SiO according to the microprobe results). Simulations show that virtually none of the beam electrons can penetrate the 200-nm-thick films. Since, in the previous specimen set, we found optimum luminescence for annealing temperatures below 500 °C, in Set B we produced different Nd concentrations (Table 1) and annealed all specimens at temperatures between 300 and 500 °C.

Fig. 3 shows the photoluminescence results for a specimen with ~0.44 at.% (~1.3×10^{20} ions/cm^{-3}) Nd, annealed at 300, 400, and 500 °C. All four principal Nd emission bands between 800 and 1400 nm were clearly observed, and the nanocluster luminescence was undetectable. All Nd spectra are well-modeled with several overlapping Gaussians (Lorentzians resulted in lower correlation coefficients). The inset to Fig. 3 shows the results of the fit for the $^4F_{3/2} \rightarrow {}^4I_{9/2}$ transition using four Gaussian curves; the result is clearly a good fit to the experimental spectra. Gaussian peaks are consistent with the inhomogenously broadened transitions expected for neodymium ions embedded in an amorphous host.

To our knowledge, this is the first time that the technically important $^4F_{3/2} \rightarrow {}^4I_{13/2}$ transition at 1350 nm has been observed in a non-resonant pumping configuration using silicon nanocluster sensitizers. The emission was strongest for the 400 °C anneals, but was only approxi-

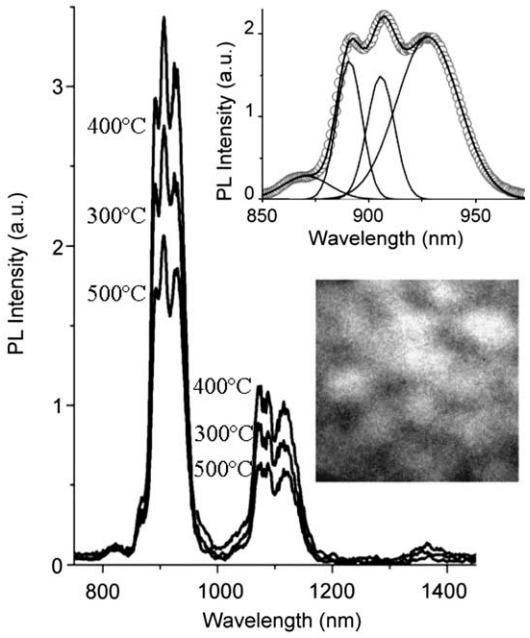

Fig. 3. Photoluminescence data for Specimen Set B (0.44 at.% Nd) annealed at 300, 400, 500 °C. Data from two spectrometers are stitched together at approximately 950 nm to display a greater range. The Gaussian fit used to determine the peaks is seen in the top inset for the $^4F_{3/2} \rightarrow {}^4I_{9/2}$ transition. An elemental map (using the Si K edge at 1839 eV) of the 500 °C anneal is shown on the bottom right (image width = 15 nm), in which bright areas correspond to silicon-rich clusters. There was no evidence of crystallinity in the electron diffraction patterns.

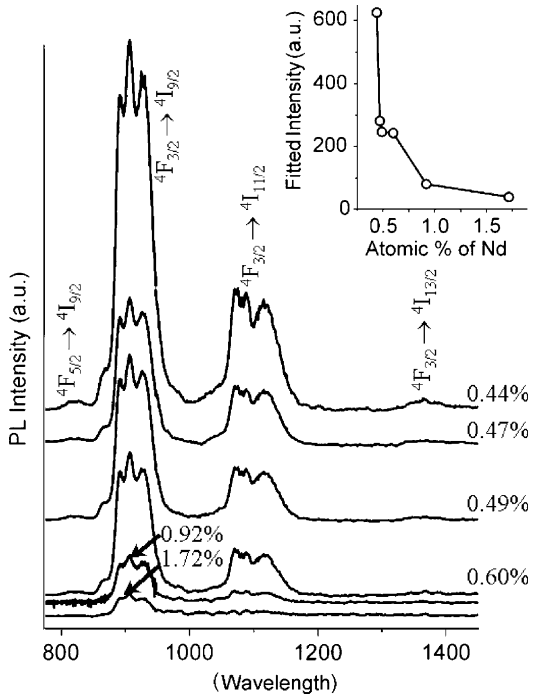

Fig. 4. Photoluminescence data for Specimen Set B for all specimens annealed at 400 °C. Data from two spectrometers are stitched together at approximately 950 nm to display a greater range. The inset shows the peak intensity of the fitted $^4F_{3/2} \rightarrow {}^4I_{9/2}$ transition as a function of Nd concentration.

mately 20% lower for the 300 °C anneals. The emission intensity was investigated for the different samples and it was greatest for the lowest Nd concentration (0.44 at.%, see Fig. 4). Concentration quenching effects are well documented in neodymium-doped glass and are due to a variety of cross-relaxation processes and Nd clustering [14]. Therefore, for silicon-rich oxide (SRO) glass with an overall composition close to SiO, the Nd concentration required to maximize the emission intensity is between 0.14 and 0.44 at.% Nd.

The fact that strong non-resonantly pumped Nd emission can be obtained at such low-processing temperatures may be useful for the fabrication of devices based on this material. Here, we demonstrate this concept using a simple metal-mirrored Fabry–Perot microcavity (one that could not be fabricated at high-annealing temperatures) in which the active material was SiO:Nd. Four separate layers were deposited on a fused quartz wafer: a 200-nm-thick Ag back mirror, the active SRO:Nd layer grown under conditions matching as closely as possible to the best sample from Set B (0.44 at.% Nd), a partly transparent 35-nm-thick Ag top mirror, and a top 50-nm-thick SiO_2 layer to serve as an oxidation barrier. The whole multilayer structure was subsequently annealed at 400 °C under the same conditions as for previous samples (we found that annealing at temperatures above 500 °C destroyed the silver mirrors, illustrating one of the advantages associated with this lower-temperature procedure).

The cavity mode depends on the optical path length of the active layer as well as the optical phase change upon reflection at the metal mirrors:

$$\lambda = \frac{4\pi n d \cos\theta}{2\pi m + \phi_1 + \phi_2}, \tag{1}$$

where λ is the wavelength, n is the refractive index of the active layer (the SOPRA tables provide the refractive indices of SiO [15]), d is the specimen thickness, θ is the emission angle (90° in the present measurements) m is the order number, and ϕ is the phase change on reflection at the SiO–Ag interfaces. In order to obtain a resonant mode at 915 nm (the peak emission band in these samples), transfer matrix calculations showed that an active layer thickness of 433 nm is required to obtain the $m = 1$ interference maximum (i.e., the *second* maximum, since the values of ϕ in Eq. (1) provide a solution for the $m = 0$ mode as well). We kept the SiO:Nd deposition conditions as similar as possible to those for the most intensely emitting specimen in Fig. 4.

The results are shown in Fig. 5. For a modest Q-factor of 135 we observe an intensity enhancement factor of an order of magnitude over the best non-cavity specimens normalized to an equivalent net material thickness. By slightly grading the SRO:Nd layer thickness using an off-axis deposition geometry the resonant wavelength could be tuned across the free space Nd emission peak at different locations on the same specimen (inset to Fig. 5). The measured intensity enhancement factor does not account for reflection and absorption of the pump beam in the top silver

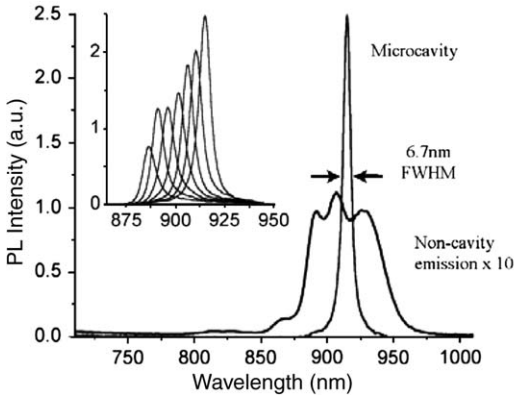

Fig. 5. Microcavity photoluminescence data. The second-order SiO:Nd 900 nm microcavity is shown, with the 0.44 at.% sample from Specimen Set B as a reference. Both were annealed at 400 °C and pumped with the 476 nm HeCd laser line. The inset displays the spectral tunability of the graded cavity.

mirror, or for multiple reflections of the laser beam inside the cavity. According to theory, the enhancement factor G, in a narrow solid angle perpendicular to the mirrors, is given by [16]:

$$G = \frac{(1+\sqrt{R_b})^2(1-R_t)}{(1-\sqrt{R_b R_t})^2}, \quad (2)$$

where R_t and R_b are the reflectivities of the top and bottom mirrors, respectively. Here, G is in effect a *rate* enhancement factor, but, following the discussion of Vredenberg et al. [16], it can be equal to the intensity enhancement if the lifetimes are similar, which is the case for the present relatively low-Q samples (data not shown). Eq. (2) gives $G = 86$, which is several times higher than the observed value of ~10. On the other hand, the measured cavity linewidth (~7 nm) is very close to the theoretical one (it is 8 nm for a 35-nm-thick Ag mirror and decreases to 6 nm for a 50-nm-thick top mirror. Here, we see a Q-factor comparable with theory but an intensity enhancement factor several times smaller. This is due to a variety of competing effects including pump beam absorption in the top mirror, multiple reflections of the pump beam in the cavity, the finite collection angle of the luminescence, and the fact that the emitters are distributed evenly throughout the active layer and are not concentrated at the electric field antinode positions as assumed in Eq. (2) [16].

4. Conclusion

We have shown that the principal neodymium emission bands can be effectively pumped via a strong non-resonant transfer mechanism from amorphous silicon nanoclusters. Temperature quenching is remarkably low, suggesting that the back-transfer processes are weak. Excellent emission characteristics can be obtained at processing temperatures as low as 300 °C. All of the principal Nd emission bands are readily identified in specimens under conditions in which there is no detectable emission in resonantly-pumped Nd-doped silica films. These observations are encouraging with respect to the development of optical devices based on SRO:Nd. To illustrate this we demonstrated a simple Fabry–Perot microcavity centered at 915 nm into which the Nd emission was coupled to produce a narrow and intense emission spectrum. Currently, we are further optimizing the specimen synthesis parameters and constructing higher-Q microcavities using dielectric mirrors, as well as using rate equation modeling of the rise and decay times in order to extract some of the critical characteristics (transfer times, cross-sections, etc.) for estimating gain and loss parameters in this material.

Acknowledgments

Financial support for this work is due to the PRF, NSERC, and iCORE. Ken Marsh and Sergei Matveev are gratefully acknowledged for technical assistance.

References

[1] A. Polman, J. Appl. Phys. 82 (1997) 1.
[2] A. Meldrum, Recent Res. Develop. Nucl. Phys. 1 (2004) 93.
[3] P.G. Kik, A. Polman, Mater. Res. Soc. Bull. 23 (4) (1998) 48.
[4] J. Lee, J.H. Shin, N. Park, J. Lightwave Technol. 23 (2005) 19.
[5] S. Seo, M.-J. Kim, J.H. Shim, Appl. Phys. Lett. 83 (2003) 2778.
[6] G. Franzo, V. Vinciguerra, F. Priolo, Appl. Phys. A 69 (1999) 3.
[7] G. Franzo, V. Vinciguerra, F. Priolo, Philos. Mag. B 80 (2000) 719.
[8] S.P. Withrow, C.W. White, A. Meldrum, J.D. Budai, D.M. Hembree Jr., J.C. Barbour, J. Appl. Phys. 86 (1999) 396.
[9] M. Glover, A. Meldrum, Opt. Mater. 27 (2005) 977.
[10] S. Cheylan, R.G. Elliman, Nucl. Instr. Meth. Phys. Res. B 148 (1999) 986.
[11] A. Hryciw, C. Blois, A. Meldrum, T. Clement, R. DeCorby, Q. Li, this issue.
[12] A. Hryciw, J. LaForge, C. Blois, M. Glover, A. Meldrum, Adv. Mater. 17 (2005) 845.
[13] D. Pacifici, G. Franzò, F. Priolo, F. Iacona, Phys. Rev. B 67 (2003) 245301.
[14] J.A. Caird, A.J. Ramponi, P.R. Staver, J. Opt. Soc. Am. B 8 (7) (1991) 1391.
[15] Available from: <http://www.sopra-sa.com/more/database.asp>.
[16] A.M. Vredenberg, N.E.J. Hunt, E.F. Schubert, D.C. Jacobson, J.M. Poate, G.J. Zydzik, Phys. Rev. Lett. 71 (1993) 517.